# TUDelft

Delft University of Technology

## Nature-based flood protection

### The efficiency of vegetated foreshores for reducing wave loads on coastal dikes

Vuik, V.; Jonkman, S. N.; Borsje, B. W.; Suzuki, T.

**Important note**
To cite this publication, please use the final published version (if applicable).
Please check the document version above.

# Nature-based flood protection: the efficiency of vegetated foreshores for reducing wave loads on coastal dikes

Vincent Vuik[1,2]*, Sebastiaan N. Jonkman[1], Bas W. Borsje[3,4], and Tomohiro Suzuki[5,1]

[1] Delft University of Technology, Civil Engineering and Geosciences, P.O. Box 5048, 2600 GA, Delft, The Netherlands

[2] HKV Consultants, P.O. Box 2120, 8203 AC, Lelystad, The Netherlands

[3] University of Twente, Water Engineering and Management, P.O. Box 217, 7500 AE Enschede, The Netherlands

[4] Deltares, P.O. Box 177, 2600 MH, Delft, The Netherlands

[5] Flanders Hydraulics Research, Berchemlei 115, 2000, Antwerpen, Belgium

*Corresponding author. E-mail address: V.Vuik@tudelft.nl

## Abstract

This paper analyses the effect of vegetation on wave damping under severe storm conditions, based on a combination of field measurements and numerical modelling. The field measurements of wave attenuation by vegetation were performed on two salt marshes with two representative but contrasting coastal wetland vegetation types: cordgrass (*Spartina anglica*) and grassweed (*Scirpus maritimus*). The former is found in salty environments, whereas the latter is found in brackish environments. The measurements have added to the range with the highest water depths and wave heights presented in the literature so far. A numerical wave model (SWAN) has been calibrated and validated using the new field data. It appeared that the model was well capable of reproducing the observed decay in wave height over the salt marsh. The model has been applied to compute the reduction of the incident wave height on a dike for various realistic foreshore configurations and hydraulic loading conditions. Additionally, the efficiency of vegetated foreshores in reducing wave loads on the dike has been investigated, where wave loads were quantified using a computed wave run-up height and wave overtopping discharge. The outcomes show that vegetated foreshores reduce wave loads on coastal dikes significantly, also for the large inundation depths that occur during storms and with the vegetation being in winter state. The effect of the foreshore on the wave loads varies with wave height to water depth ratio on the foreshore. The presence of vegetation on the foreshore extends the range of water depths for which a foreshore can be applied for effective reduction of wave loads, and prevents intense wave breaking on the foreshore to occur. This research demonstrates that vegetated foreshores can be

considered as a promising supplement to conventional engineering methods for dike reinforcement.

## 1    Introduction

Integration of ecosystems in coastal protection schemes is increasingly mentioned as a valuable supplement to conventional engineering methods (Jones et al., 2012; Temmerman et al., 2013; Van Wesenbeeck et al., 2014). Coastal ecosystems like sand dunes can fulfil the same function as man-made flood defences, such as dikes and dams. Other ecosystem types, such as salt marshes (e.g. King and Lester, 1995; Möller et al., 1999; Möller and Spencer, 2002; Möller, 2006; Arkema et al., 2013), intertidal flats and mangrove forests (e.g. Mazda et al., 2006; Quartel et al., 2007; Horstman et al., 2014) can potentially be used as foreshore protection to reduce the impact of storm surges and wind waves on the flood defences (Borsje et al., 2011; Gedan et al., 2010; Sutton-Grier et al., 2015). This paper focuses on the latter ecosystem types: vegetated foreshores in front of coastal dikes (Figure 1), since this system has only received limited attention in the literature, despite of the potential of this type of ecosystems to directly affect the flood risk in the area behind the flood defence.

A vegetated foreshore consists of a sediment body, covered with vegetation, in front of a dike. Surface waves, propagating from deep water towards a coastal dike, can significantly lose energy when a vegetated foreshore is present, due to depth-induced wave breaking, bottom friction and wave attenuation by vegetation. Wave run-up on the outer slope of coastal dikes is governed by the incident wave height and wave period. When the wave run-up exceeds the crest height of the dike, wave overtopping over the dike occurs. This might ultimately lead to erosion of the inner slope and breaching of the dike. Both wave run-up and wave overtopping discharge directly depend on the incoming wave height, which means that the presence of a vegetated foreshore influences the likelihood of dike breaching due to wave overtopping.

**Westkapelle, sandy foreshore, North Sea**
Foreshore elevation 4.0 m+NAP, slope 1:40
Dike height 12.6 m+NAP, slope 1:6
Design conditions: h = 4.9 m+NAP, $H_{m0}$ = 4.6 m, $T_{m-1,0}$ = 9 s

**Hellegat, salt marsh, Western Scheldt**
Marsh elevation 3.0 m+NAP, width 200 m, slope 1:40
Dike height 9.5 m+NAP, slope 1:4
Design conditions: h = 6.0 m+NAP, $H_{m0}$ = 1.9 m, $T_{m-1,0}$ = 5 s

**Groningen, salt marsh, Wadden Sea**
Marsh elevation 2.0 m+NAP, width 800 m, slope 1:750
Dike height 9.1 m+NAP, slope 1:4
Design conditions: h = 5.3 m+NAP, $H_{m0}$ = 1.8 m, $T_{m-1,0}$ = 5 s

**Texel, salt marsh Schorren, Wadden Sea**
Marsh elevation 1.8 m+NAP, width 400 m, slope 1:250
Dike height 6.9 m+NAP, slope 1:3
Design conditions: h = 4.4 m+NAP, $H_{m0}$ = 1.4 m, $T_{m-1,0}$ = 5 s

*Figure 1 – Examples of foreshores in the Netherlands and their characteristics: sandy foreshore near West-kapelle sea defence, bordering the North Sea (upper left), natural salt marsh Hellegatpolder in the Western Scheldt (upper right), man-made salt marsh along the Wadden Sea dikes of Groningen province (lower left), salt marsh Schorren at the Wadden Sea side of the barrier island Texel, with marsh edge protection (lower right). Source: https://beeldbank.rws.nl, Rijkswaterstaat. The numbers in this figure will be explained and used in section 4.*

3

The first process that leads to wave energy reduction on vegetated foreshores is depth-induced wave breaking (Battjes and Janssen, 1978; Duncan, 1983) on the shallow foreshore in front of the dike. The maximum possible wave height depends primarily on the water depth. The ratio between both is the dimensionless breaker parameter. Several studies explain how the breaker parameter can vary due to differences in offshore wave steepness (e.g. Battjes and Stive, 1985; Nairn, 1990), bottom slope (e.g. Nelson, 1994) or wave length (Ruessink et al., 2003). For a (nearly) horizontal bottom, the height of individual waves in a naturally occurring random wave train is at maximum 55 percent of the water depth (Massel, 1996; Nelson, 1994). On steep slopes, higher values can be found.

Additionally, wave energy can be dissipated by bottom friction on shallow foreshores with a surface covered with for instance vegetation, shells or sand ripples. Padilla-Hernández and Monbaliu (2001) have compared the capability of different bottom friction formulations in reproducing wave measurements in shallow water conditions, and argue that formulations for dissipation by bottom friction, like the models by Madsen et al. (1988) or Weber (1989), which explicitly take physical parameters for bottom roughness into account, should be preferred in wave modelling in shallow water areas.

And third, surface waves propagating through vegetation fields lose energy when they perform work on vegetation stems, branches and leaves (Dalrymple et al., 1984). This results in a decrease in wave height. Understanding wave attenuation by vegetation is crucial for determining the efficiency of vegetated foreshores in reducing wave loads on coastal dikes. Therefore, as part of this research, an inventory has been made of available studies that give insight in wave attenuation by vegetation (Figure 2). Most of these studies are based on field or laboratory experiments with water depths of below one meter and/or wave heights of typically 10 to 30 centimetres.
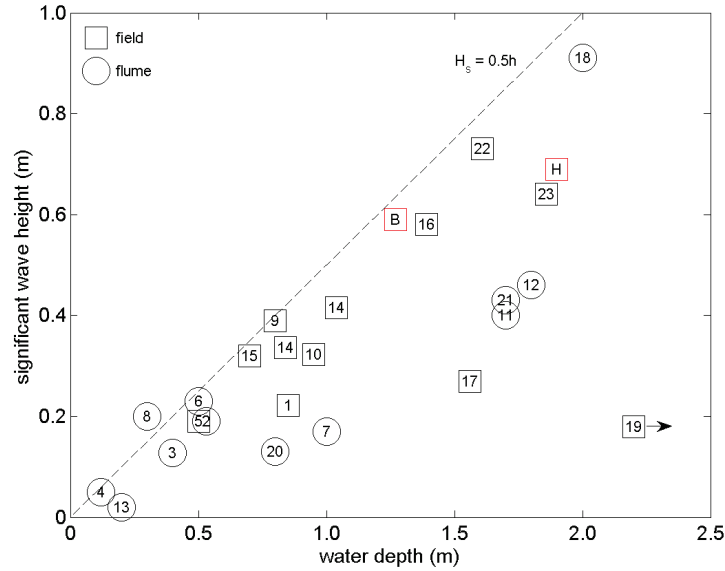
*Figure 2 – Maximum water depth and significant wave height, as reported for experiments with wave attenuation by vegetation. For regular waves, the plot position is determined by a computed equivalent significant wave height, using $H_s = 1.41H$. The dotted line roughly indicates depth-limitation due to breaking. Studies included: see Table 1. The letters H and B belong to the field measurements described in the current paper at the salt marshes Hellegat and Bath, respectively (section 2).*

*Table 1 – Studies included in Figure 2, their characteristics, maximum water depth and maximum regular or significant wave height. Numbers indicated with an asterisk (\*) are based on estimation.*

| # | Publication | Characteristics | max h | max H | max $H_s$ |
|---|-------------|-----------------|-------|-------|-----------|
| 1 | Allen et al. (2008) | Field, *bulrush* | 0.85 | | 0.22* |
| 2 | Anderson and Smith (2014) | Flume, synthetic plants | 0.53 | | 0.19 |
| 3 | Augustin et al. (2009) | Flume, wooden pens & polyethylene | 0.40 | 0.09 | |
| 4 | Bouma et al. (2005) | Flume, *Spartina anglica, Zostera noltii* | 0.12 | 0.05 | |
| 5 | Cooper (2005) | Field, salt marsh species | 0.50 | | 0.19 |
| 6 | Coops et al. (1996) | Artificial wave basin, *Phragmites & Scirpus* | 0.50 | 0.23 | |
| 7 | Dubi and Torum (1996) | Flume, synthetic plants | 1.00 | | 0.17 |
| 8 | Fonseca and Cahalan (1992) | Flume, 4 plant species | 0.30 | 0.20 | |
| 9 | Jadhav et al. (2013) | Field, *Spartina alterniflora* | 0.80 | | 0.39 |
| 10 | Knutson et al. (1982) | Field, *Spartina alterniflora* | 0.95 | | 0.32* |
| 11 | Koftis et al. (2013) | Flume, polypropylene stripes | 1.70 | | 0.40 |
| 12 | Manca et al. (2012) | Flume, polypropylene stripes | 1.80 | | 0.46 |
| 13 | Mei et al. (2011) | Flume, perspex cylinders | 0.20 | 0.02 | |
| 14 | Möller and Spencer (2002) | Field, salt marsh species | 1.04 | | 0.42* |
| 15 | Möller (2006) | Field, salt marsh species | 0.70 | | 0.32 |
| 16 | Möller et al. (1999) | Field, salt marsh species | 1.39 | | 0.58 |
| 17 | Möller et al. (2011) | Field, *Phragmites australis* | 1.56 | | 0.27 |
| 18 | Möller et al. (2014) | Flume, 3 salt marsh species | 2.00 | | 0.91 |
| 19 | Paul and Amos (2011) | Field, *Zostera noltii* | 3.50 | | 0.18 |
| 20 | Sánchez-González et al. (2011) | Flume, synthetic plants | 0.80 | | 0.13 |
| 21 | Stratigaki et al. (2011) | Flume, polypropylene stripes | 1.70 | 0.43 | |
| 22 | Yang et al. (2012) | Field, *Scirpus & Spartina alterniflora* | 1.61 | | 0.73 |
| 23 | Ysebaert et al. (2011) | Field, *Spartina alterniflora & S. mariqueter* | 1.86 | | 0.64 |
| H | This study, Hellegat | Field, *Spartina anglica* | 1.90 | | 0.69 |
| B | This study, Bath | Field, *Scirpus maritimus* | 1.27 | | 0.59 |

5

Wave attenuation does not only depend on vegetation properties like vegetation height, stem diameter and spacing, but also on hydraulic characteristics such as the wave height, the water depth (e.g. Möller et al., 1999; Möller et al., 2014) and ambient currents (Hu et al., 2014). Therefore, wave attenuation rates measured in moderate conditions cannot be applied directly to severe storm conditions, and physical or semi-empirical modelling approaches are required for estimating the wave damping capacity of vegetated foreshores under these more extreme circumstances.

One modelling approach for describing the effect of vegetation on wave propagation is to apply an increased bottom friction coefficient (e.g. Möller et al., 1999). The main drawback of this approach is the absence of information about vegetation height. Therefore, most modelling approaches make use of a cylinder approach (Dalrymple et al., 1984; Mendez and Losada, 2004), estimating the wave-induced drag force exerted on the vegetation stems, and optionally also on root systems or branches. This type of model relies on knowledge of the bulk drag coefficient $C_D$, representing drag that is due to pressure differences and drag that is due to skin friction, but also processes that are not captured by the physical model, for example plant swaying (Dijkstra and Uittenbogaard, 2010; Méndez et al., 1999; Mullarney and Henderson, 2010; Riffe et al., 2011), attenuation of orbital motion by the vegetation canopy (Pujol et al., 2013) and interaction between individual wakes in dense vegetation fields (Suzuki and Arikawa, 2011). Because of the complex physics underlying the bulk drag coefficient $C_D$, a-priori determination of an appropriate value for a certain vegetation species and hydrodynamic conditions is precluded, and site-specific calibration of $C_D$ is required. However, several authors have attempted to relate $C_D$ to the Reynolds number $Re$ (Kobayashi et al., 1993; Méndez et al., 1999; Pinsky et al., 2013) or to the Keulegan-Carpenter number $K$ (Mendez and Losada, 2004). Bradley and Houser (2009) and Anderson and Smith (2014) found no improvement when $C_D$ was parameterized with $K$ instead of $Re$. Coefficients in these relations are mostly obtained by calibration.

Formulations for vegetation bulk drag coefficients vary considerably in the literature (Table 2). Theoretically, drag coefficients of a smooth, rigid cylinder has a value of about 1.0-1.2 for sub-critical flow. However, it is difficult to estimate an appropriate bulk drag coefficient in wave conditions for different shapes, densities and flexibilities (Suzuki,

2011). Most studies that analyse bulk drag coefficients present a computed value that is based on observed wave attenuation. An exception is the study of Hu et al. (2014), where drag forces were directly measured. Because the bulk drag coefficient is usually a result of computations, it also reflects all processes that are not or incorrectly captured in the model involved.

Table 2 – Relations between Reynolds number Re and bulk drag coefficient $C_D$ presented in the literature, based on a combination of a certain (synthetic or natural) vegetation type, vegetation height $l_v$, vegetation diameter $b_v$, water depth h and wave height H (regular waves) or $H_s$ (irregular waves). The last column gives a comparison of the result for Re = 1000, which is a typical number for storm conditions at the measurement sites in the current study.

| Publication | Vegetation properties | Description of $C_D$ | Based on range | $C_D$ for Re = 1000 |
|---|---|---|---|---|
| Méndez et al. (1999) | Flexible plastic strips 52x0.03 mm (Asano et al., 1992), $l_v$=0.25 m, h≈0.50 m, H≤0.12 m | $C_D = (2200/Re)^{2.2} + 0.08$ | 200<Re<15500 | $C_D$ = 5.75 |
| Paul and Amos (2011) | Zostera noltii, sea grass, $l_v$=0.13 m, h=1.5-3.5 m, $H_s$=0.10-0.18 m | $C_D = (153/Re)^{1.45}+0.06$ | 100<Re<1000 | $C_D$ = 0.13 |
| Jadhav and Chen (2012) | Spartina alterniflora, $l_v$=0.63 m, $b_v$=8 mm, h≈0.4-0.6 m, $H_s$≤0.4 m | $C_D = 2,600/Re+0.36$ | 600<Re<3200 | $C_D$ = 2.96 |
| Pinsky et al. (2013) | Statistical analysis of attenuation by several salt marsh vegetation species | $\log(C_D)= \beta_0+\beta_1\log(c·Re)$ $c=3·10^{-4}$, $\beta_0$=-1.72, $\beta_1$=-1.67 | not specified | $C_D$ = 0.14 |
| Anderson and Smith (2014) | Synthetic Spartina, $l_v$=0.42 m, $b_v$=6.4 mm, h=0.31-0.53 m, $H_s$=0.05-0.19 m | $C_D = (744/Re)^{1.27}+0.76$ | 500<Re<2300 | $C_D$ = 1.45 |
| Hu et al. (2014) | Stiff wooden rods, $l_v$=0.36 m, $b_v$=10 mm, h=0.25-0.50 m, H=0.04-0.20 m | $C_D = (730/Re)^{1.37}+1.04$ | 300<Re<4700 | $C_D$ = 1.69 |
| Möller et al. (2014) | Predominantly Elymus athericus, $l_v$=0.70 m, $b_v$=1.3 mm, h=2.0 m, $H_s$=0.1-0.9 m | $C_D = (227/Re)^{1.62}+0.16$ | 100<Re<1100 (estimated) | $C_D$ = 0.25 |

A calibrated relation between Re and $C_D$ is generally used to estimate bulk drag coeffi-cients under highly turbulent storm conditions, which are characterized by high Reynolds numbers. By using extrapolation to higher Reynolds numbers, possible physical thresh-olds are implicitly neglected, for example thresholds for swaying of vegetation (Bradley and Houser, 2009; Méndez et al., 1999; Möller et al., 2014; Rupprecht et al., 2015) or

7

vegetation collapse by uprooting or stem breakage (Liffen et al., 2013; Möller et al., 2014; Puijalon et al., 2011; Seymour and Tegner, 1989). Additionally, seasonal variations in aboveground biomass and mechanical fragility can considerably influence wave damping capacity (Bouma et al., 2014; Paul and Amos, 2011).

As aforementioned, many authors describe the potential of vegetated foreshores for coastal protection. However, the capability of these ecosystems in serving as protection during extreme storm conditions with high waves and large water depths is not well understood. Most studies of wave attenuation by vegetation concern field or laboratory experiments with small water depths and low wave heights (Figure 2). This means that most existing measurements are not directly suitable for drawing conclusions about the behaviour of vegetation under conditions that are relevant to the design of coastal dikes: hydrodynamic conditions with severe waves and water depths of several meters.

Empirical formulas and process-based descriptions of wave attenuation are mostly applied for bridging the gap between measured conditions and extreme conditions. These instruments are mainly based on measurements carried out during low-energy conditions (Anderson et al., 2011), which leads to uncertainties when applying them to storm conditions. This is reflected by the large variability in formulations that describe the drag coefficient as a function of wave properties and vegetation characteristics (Table 2).

Understanding the effect of vegetation on wave damping under storm conditions is for utmost importance to come up with design criteria for dikes with vegetated foreshores in front. The actual consequences of wave reduction by vegetated foreshores for hydraulic loads on dikes have never been quantified in the literature. Therefore the aim of this paper is to provide understanding of the efficiency of vegetated foreshores for reducing wave run-up on and wave overtopping over coastal dikes. This insight is obtained utilizing a combination of field measurements and numerical modelling. New field measurements were required, because existing detailed field observations of storm wave attenuation by a characteristic north-west European vegetation canopy were absent. The new field data has been used to calibrate and validate a numerical model that simulates wave attenuation over vegetated foreshores. This model has been applied to some representative examples taken from the Netherlands, to show how and how much vegetat-

ed foreshores in front of coastal dikes can reduce wave loads on a dike under severe storm conditions.

This paper is organised as follows. The field measurements are discussed in section 2. Section 3 describes the numerical modelling work on wave energy dissipation over vegetated foreshores. Section 4 shows the results of the application of the numerical model, to illustrate how much vegetated foreshores can affect the wave loads on dikes for some typical examples taken from the Netherlands. The paper closes with a discussion and conclusions in the sections 5 and 6.

## 2   Field measurements

A field measurement campaign has been carried out, in which wave attenuation over vegetated foreshores has been measured during severe storms in the Netherlands in the months November 2014 till January 2015. The measurements have been performed on two salt marshes with two representative but contrasting coastal wetland vegetation types: cordgrass (*Spartina anglica*) and grassweed (*Scirpus maritimus*). The former is found in salty environments, whereas the latter is found in brackish environments. The obtained data set has been used for the calibration and validation of a numerical model that describes wave propagation over vegetated foreshores (section 3).

### 2.1 Wave measurement configuration

Field measurements were carried out at two exposed salt marshes in the Western Scheldt estuary in the Netherlands. Wave gauges were deployed between November 23rd 2014 and January 21st 2015 at the salt marshes Hellegat and Bath (Figure 3). The marsh Hellegat is covered with the salt-tolerant *Spartina anglica* (Common Cordgrass). Mixed vegetation is present on the higher marsh, but this is beyond the area where the wave gauges were deployed. At Bath, the discharge of the Scheldt river causes a brackish environment, which is what accounts for the dominance of *Scirpus maritimus* (Alkali Bulrush) at the measurement site. The tidal range in the Western Scheldt increases from approximately 4 m at the estuary mouth to 5 m at Bath. Under severe storm conditions, both storm surge and wind waves can penetrate from the North Sea into the estuary. Significant inundation of the higher areas of the salt marsh only occurs when there is a combination of high tide and storm surge.

9

At both marshes, four wave gauges (Ocean Sensor Systems, Inc., USA) were deployed in the same configuration. One sensor was placed on the mudflat, directly in front of the marsh edge (S1). The three other sensors (S2, S3 and S4) were located in the vegetation, at distances of 5, 15 and 50 m from the marsh edge (Figure 4). The elevation heights were determined using an RTK-GPS device with a precision in the order of 1 cm.

The wave gauges were programmed to record the pressure with a frequency of 5 Hz over a period of 7 minutes, every 15 minutes. This means that every burst contains 2100 samples. The measured pressure is the result of the local atmospheric pressure, the hydrostatic pressure and the dynamic wave pressure. In the post-processing, these three components were separated. The hydrostatic pressure provides information about the still water level, whilst the dynamic wave pressure depends on the surface waves. In the conversion of dynamic wave pressures to variations in the surface elevation due to waves, depth-attenuation of the pressure signal according to linear wave theory was taken into account. The pressure sensors were mounted approximately 0.10 m above the sediment surface.
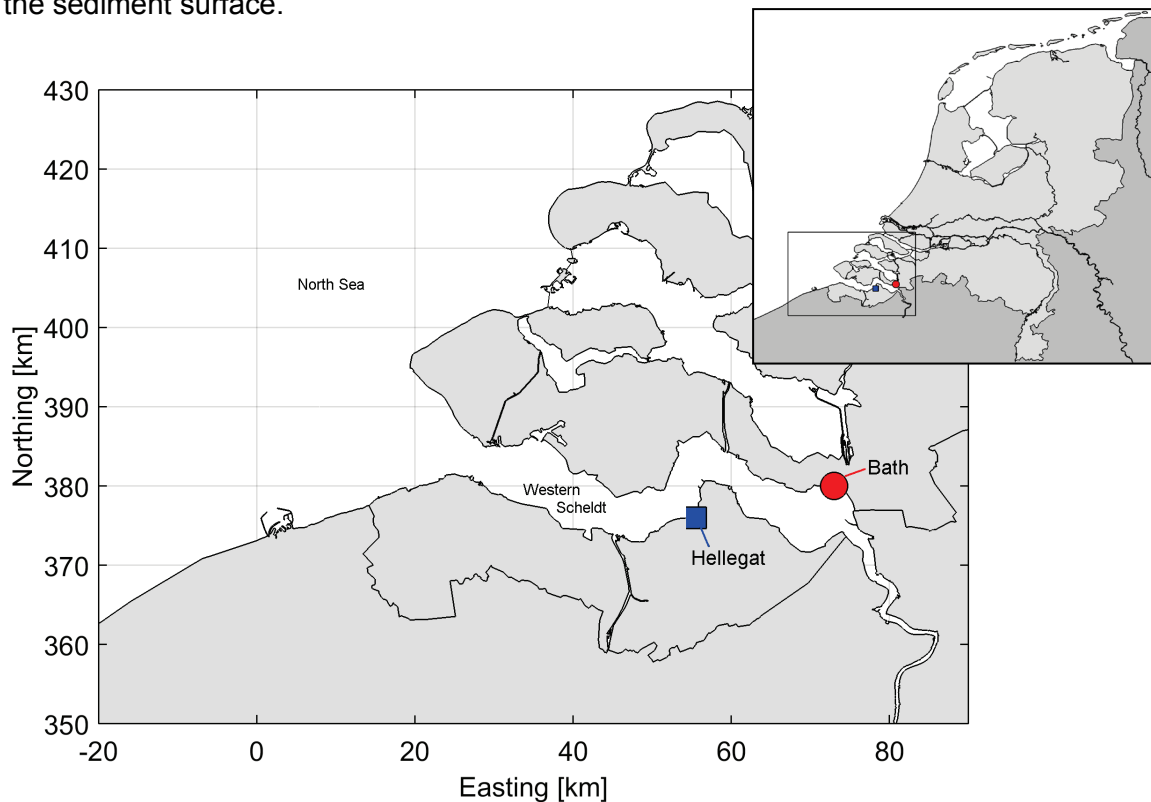


Figure 3 – Location of the salt marshes Hellegat and Bath in the Western Scheldt estuary, the Netherlands
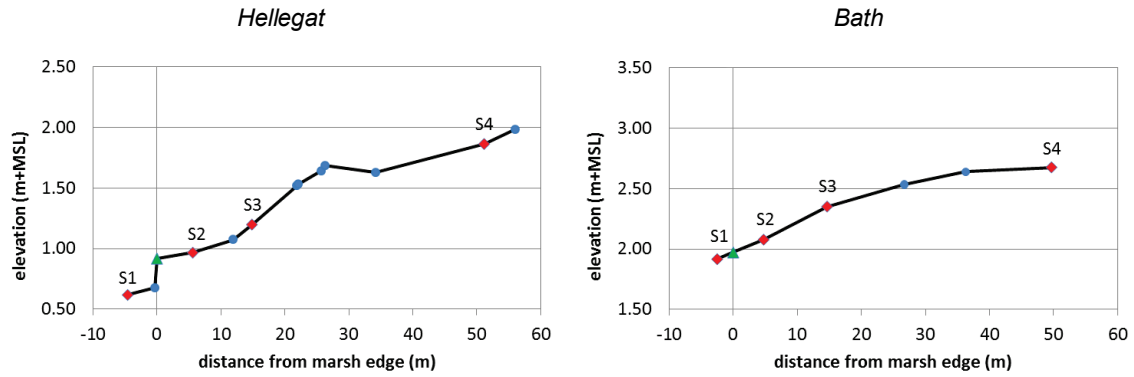
Figure 4 – Bathymetric measurements at wave gauge locations S1-S4 (red diamonds) and at some additional points (blue circles) at Hellegat (left) and Bath (right). The green triangle shows the position of the marsh edge.

## 2.2 Vegetation measurements

Vegetation properties were determined by measuring the length, the diameter at the top, the diameter in the middle and the diameter at the base of individual stems. At Bath, the properties of all plants within a surface area of 0.5x0.5 m were investigated between sensors S1 and S2 and between sensors S2 and S3. This area was reduced to 0.25x0.25 m for the sampling between sensors S3 and S4 because of the high stem density. At Hellegat, an area of 0.25x0.25 m was used for all samples. The vegetation samples were collected on November 19th 2014, which means that vegetation was in its winter state (Figure 5).
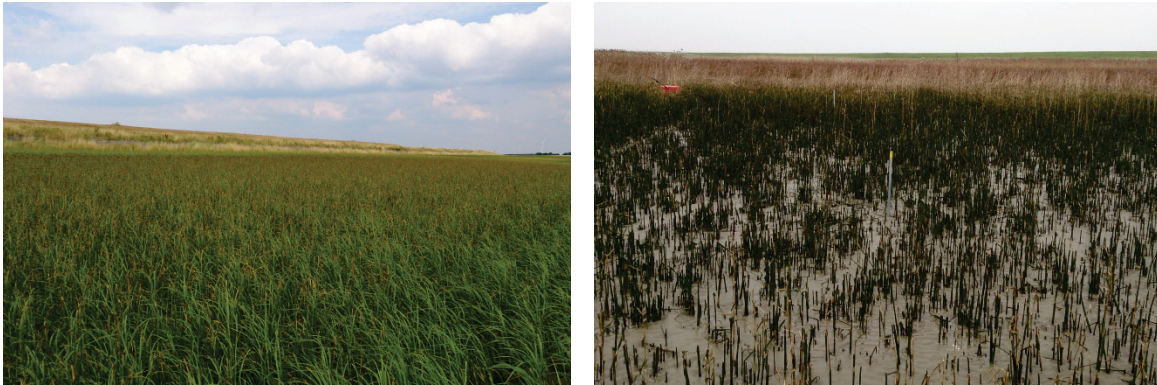


Figure 5 –Scirpus maritimus at Bath, Western Scheldt, the Netherlands in July 2014 (left) and November 2014 (right)

The *Spartina anglica* at Hellegat had a mean height $h_{mean}$ ranging from 0.20 m at the marsh edge to 0.29 m further into the vegetation field (Table 3). A near-bottom stem density $N_{v,0}$ of nearly 1000 stems/m$^2$ was present near the marsh edge, while a density

11

of more than 1500 stems/m$^2$ was found between sensors S3 and S4. The near-bottom stem diameter $b_{v,0}$ was fairly constant at approximately 3 mm. The impact of wind and waves on the vegetation in its fragile winter state was more distinct at Bath. Near the marsh edge, the dense *Spartina anglica* that was present in summer has depreciated to broken stems with a mean height of approximately 0.15 m (Figure 5). Between sensors S3 and S4, the disruption was less: the stem density, mean height and maximum height were all significantly larger than at the marsh edge. Remarkably, the mean stem diameter decreases from 8.7 mm at the marsh edge to 4.9 mm between sensors S3 and S4. The total biomass density *M* was estimated by multiplication of $h_{mean}$, $N_{v,0}$ and the near-bottom surface area $A_{v,0} = \pi b_{v,0}^2/4$.

*Table 3 – Maximum plant height $h_{max}$, mean plant height $h_{mean}$, near-bottom stem density $N_{v,0}$, mean near-bottom stem diameter $b_{v,0}$ and total biomass density M (m$^3$/m$^2$) for six sampling locations.*

| Sample | $h_{max}$ (m) | $h_{mean}$ (m) | $N_{v,0}$ (stems/m$^2$) | $b_{v,0}$ (mm) | M (m$^3$/m$^2$) |
|---|---|---|---|---|---|
| Hellegat S1-S2 | 0.61 | 0.20 | 944 | 3.0 | $1.3 \cdot 10^{-3}$ |
| Hellegat S2-S3 | 0.78 | 0.29 | 1136 | 3.4 | $3.0 \cdot 10^{-3}$ |
| Hellegat S3-S4 | 0.84 | 0.27 | 1520 | 2.7 | $2.3 \cdot 10^{-3}$ |
| Bath S1-S2 | 0.48 | 0.17 | 144 | 8.7 | $1.5 \cdot 10^{-3}$ |
| Bath S2-S3 | 0.52 | 0.15 | 372 | 8.0 | $2.8 \cdot 10^{-3}$ |
| Bath S3-S4 | 1.23 | 0.35 | 1072 | 4.9 | $7.1 \cdot 10^{-3}$ |

## 2.3 Wave characteristics

Wave conditions and water depths were measured during 115 tides between November 23$^{rd}$ 2014 and January 21$^{st}$ 2015 (Figure 6). Inundation of the full transect only takes place during storms or spring tides. In the measurement period, this happened during 88 tidal cycles at Hellegat, and during 49 tidal cycles at Bath.
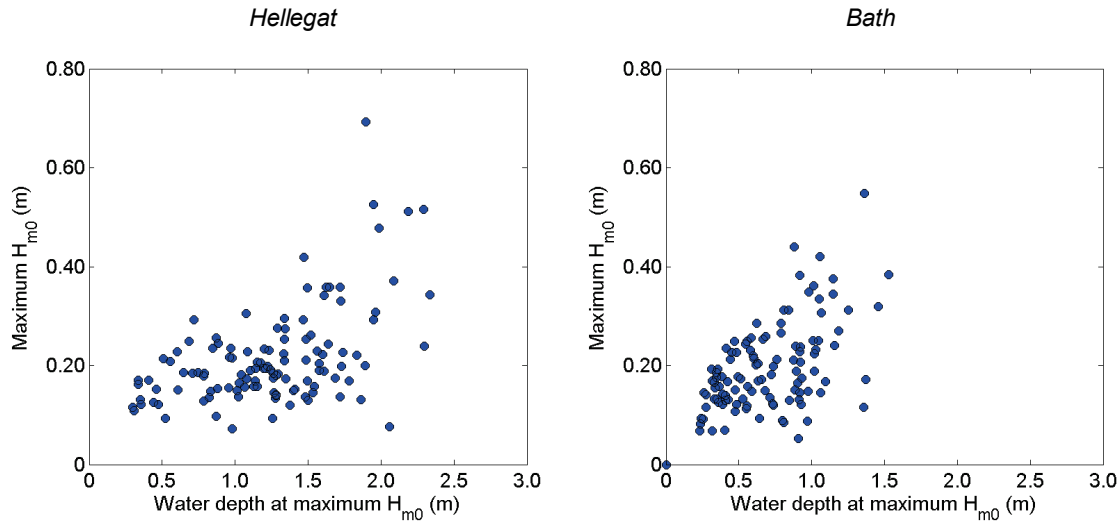
*Figure 6 – Maximum significant wave height per tide and corresponding water depth at sensor S1, on the mud flat near the marsh edge of Hellegat (left) and Bath (right) for 115 tides between November 23rd 2014 and January 21st 2015.*

The wave height can be limited by depth, wind speed or wind direction. At Hellegat, both maximum water depths and maximum exposure to waves occurs at Western or North-Western winds. Therefore, at this site, the maximum wave height (Table 4) as well as the maximum water depth (Table 6) were recorded during the Western storm of January 11th 2015, although not at exactly the same time. The maximum significant wave height at Hellegat was equal to 0.69 m, with a corresponding water depth at the marsh edge of 1.90 m (Figure 2). Wave conditions at Bath are at a maximum under South-Western wind conditions. This means that the wind direction that generates the maximum surge (NW) does not coincide with the wind direction that generates the largest waves (SW). The maximum significant wave height at Bath was equal to 0.55 m (Table 5), with a corresponding water depth at the marsh edge of 1.36 m (Figure 2).

During storms, wave peak periods $T_p$ were typically in the range of 2.5 to 4.0 seconds at Hellegat, and between 2.5 and 3.5 seconds at Bath. At these two sites in the Western Scheldt, the fraction of wave energy in the infragravity wave band (0.005 Hz < f < 0.05 Hz) was less than 1 percent during severe storms.

*Table 4 – Five tides with the largest wave height at station S1 with corresponding wave heights and water depths at all stations S1-S4 for Hellegat*

| tide | time | H$_{m0}$ S1 | H$_{m0}$ S2 | H$_{m0}$ S3 | H$_{m0}$ S4 | h S1 | h S2 | h S3 | h S4 |
|------|------|-------------|-------------|-------------|-------------|------|------|------|------|
| 96 | 11-01-2015 7:30 | 0.69 | 0.61 | 0.52 | 0.29 | 1.90 | 1.53 | 1.26 | 0.66 |
| 54 | 20-12-2014 14:00 | 0.53 | 0.46 | 0.39 | 0.21 | 1.95 | 1.58 | 1.31 | 0.70 |
| 58 | 22-12-2014 15:00 | 0.52 | 0.47 | 0.38 | 0.29 | 2.29 | 1.93 | 1.65 | 1.05 |
| 95 | 10-01-2015 17:45 | 0.51 | 0.46 | 0.40 | 0.29 | 2.19 | 1.82 | 1.56 | 0.94 |
| 94 | 10-01-2015 6:30 | 0.48 | 0.46 | 0.39 | 0.21 | 1.99 | 1.62 | 1.35 | 0.74 |

*Table 5 – Five tides with the largest wave height at station S1 with corresponding wave heights and water depths at all stations S1-S4 for Bath*

| tide | time | H$_{m0}$ S1 | H$_{m0}$ S2 | H$_{m0}$ S3 | H$_{m0}$ S4 | h S1 | h S2 | h S3 | h S4 |
|------|------|-------------|-------------|-------------|-------------|------|------|------|------|
| 94 | 10-01-2015 6:30 | 0.55 | 0.48 | 0.41 | 0.17 | 1.36 | 1.19 | 0.93 | 0.64 |
| 38 | 12-12-2014 6:30 | 0.44 | 0.36 | 0.23 | 0.00 | 0.88 | 0.73 | 0.43 | 0.00 |
| 100 | 13-01-2015 7:15 | 0.42 | 0.40 | 0.31 | 0.05 | 1.06 | 0.90 | 0.60 | 0.32 |
| 58 | 22-12-2014 15:30 | 0.38 | 0.34 | 0.29 | 0.15 | 1.43 | 1.26 | 0.98 | 0.69 |
| 92 | 09-01-2015 6:00 | 0.38 | 0.35 | 0.25 | 0.02 | 0.92 | 0.75 | 0.48 | 0.23 |

*Table 6 – Five tides with the largest water depth at station S1 with corresponding wave heights and water depths at all stations S1-S4 for Hellegat*

| tide | time | H$_{m0}$ S1 | H$_{m0}$ S2 | H$_{m0}$ S3 | H$_{m0}$ S4 | h S1 | h S2 | h S3 | h S4 |
|------|------|-------------|-------------|-------------|-------------|------|------|------|------|
| 96 | 11-01-2015 6:00 | 0.27 | 0.29 | 0.28 | 0.24 | 2.52 | 2.16 | 1.88 | 1.27 |
| 94 | 10-01-2015 5:15 | 0.31 | 0.31 | 0.31 | 0.24 | 2.41 | 2.05 | 1.78 | 1.17 |
| 95 | 10-01-2015 18:15 | 0.46 | 0.43 | 0.40 | 0.31 | 2.36 | 2.00 | 1.73 | 1.12 |
| 58 | 22-12-2014 14:30 | 0.38 | 0.38 | 0.33 | 0.23 | 2.34 | 1.98 | 1.71 | 1.10 |
| 59 | 23-12-2014 2:45 | 0.34 | 0.32 | 0.28 | 0.23 | 2.33 | 1.97 | 1.70 | 1.09 |

*Table 7 – Five tides with the largest water depth at station S1 with corresponding wave heights and water depths at all stations S1-S4 for Bath*

| tide | time | H$_{m0}$ S1 | H$_{m0}$ S2 | H$_{m0}$ S3 | H$_{m0}$ S4 | h S1 | h S2 | h S3 | h S4 |
|------|------|-------------|-------------|-------------|-------------|------|------|------|------|
| 96 | 11-01-2015 6:45 | 0.22 | 0.21 | 0.21 | 0.14 | 1.59 | 1.43 | 1.13 | 0.84 |
| 58 | 22-12-2014 15:15 | 0.35 | 0.36 | 0.32 | 0.17 | 1.57 | 1.40 | 1.10 | 0.81 |
| 94 | 10-01-2015 5:45 | 0.46 | 0.42 | 0.37 | 0.20 | 1.55 | 1.39 | 1.09 | 0.80 |
| 62 | 24-12-2014 16:45 | 0.17 | 0.15 | 0.13 | 0.07 | 1.48 | 1.32 | 1.03 | 0.73 |
| 64 | 25-12-2014 17:30 | 0.11 | 0.10 | 0.12 | 0.07 | 1.46 | 1.30 | 1.01 | 0.71 |

Waves lose energy by depth-induced wave breaking, bottom friction and wave dissipation by vegetation. These processes all depend on the wave height to water depth ratio. The water depth on the salt marshes Hellegat and Bath decreases along the transects (Figure 4). The reduction in significant wave height between the sensors S1 and S4 predominantly depends on incoming wave height and water depth (Figure 7). For identical combination of wave height and water depth, the reduction in wave height was larger at Bath than at Hellegat, despite of the larger difference in water depth between both ends of the transect at Hellegat. This difference is probably caused by the relatively high biomass density present at Bath (Table 3).
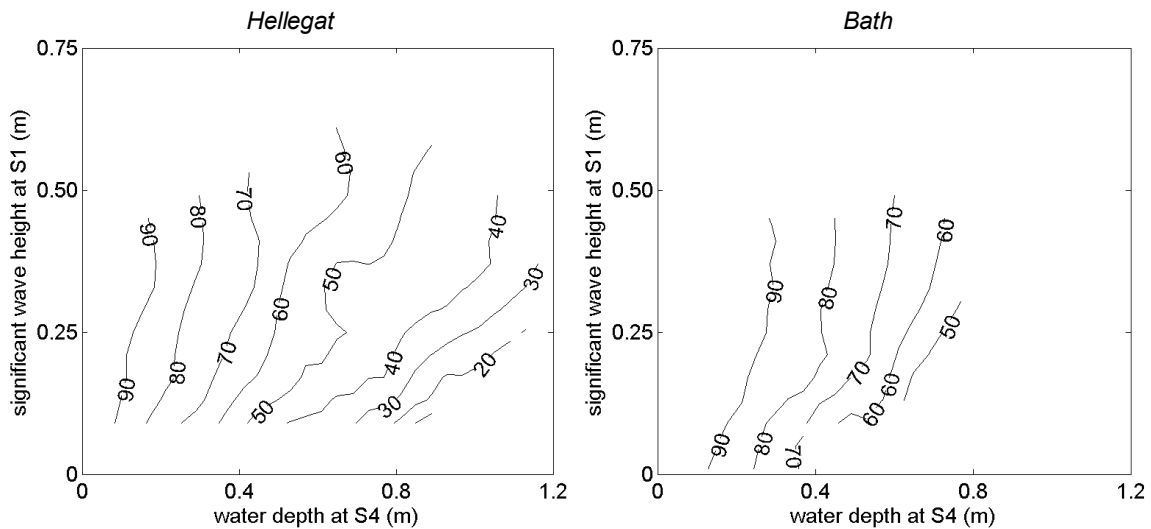


Figure 7 – Reduction in significant wave height $H_{m0}$ (%) over a distance of 50 m between sensor S1 and S4, depending on the lowest water depth over the transect at sensor S4 (horizontal axis), and the incoming wave height at sensor S1 (vertical axis) for Hellegat (left) and Bath (right).

## 3    Numerical modelling of wave propagation over vegetated foreshores

To be able to distinguish between the processes of wave breaking, bottom friction and wave attenuation by vegetation, a numerical modelling investigation has been carried out. This section describes the modelling approach, calibration, validation and application of the model.

### 3.1 Modelling approach

The measurements of wave propagation over vegetated foreshores have been reproduced with the spectral wave model SWAN (Simulating WAves Nearshore, Booij et al., 1999; Ris et al., 1999). The SWAN model includes the depth-induced wave breaking model of Battjes and Janssen (1978), different formulations for bottom friction, including

15

Madsen et al. (1988), and the method for accounting wave damping by vegetation developed by Mendez and Losada (2004). Suzuki et al. (2012) validated the performance of the vegetation module of SWAN. Additionally, they enabled schematization of vertical differences in vegetation characteristics in the model by specifying multiple layers. SWAN is capable of reproducing energy dissipation in shallow water, as long as the amount of long wave energy is limited. Total energy dissipation (i.e. wave heights) can be simulated relatively accurately with SWAN, compared to the simulation of the spectral shape (i.e. wave periods) (Van Gent and Doorn, 2001).

Three data sets were used for model calibration and validation: the data from Hellegat and Bath, described in this paper, and wave data from a salt marsh covered with *Spartina alterniflora* (Smooth Cordgrass) at East Chongming island, China, reported in Yang et al. (2012). For the calibration and validation of the SWAN model, the bathymetry of the field sites (Figure 4) was included in an 1D model schematization, with a resolution of 0.5 m. The significant wave height $H_{m0}$ and mean wave period $T_{m01}$ measured at the first sensor were used to define the incoming Jonswap wave spectrum. The measured significant wave heights at the other sensors were compared with the corresponding model outcomes during calibration and validation.
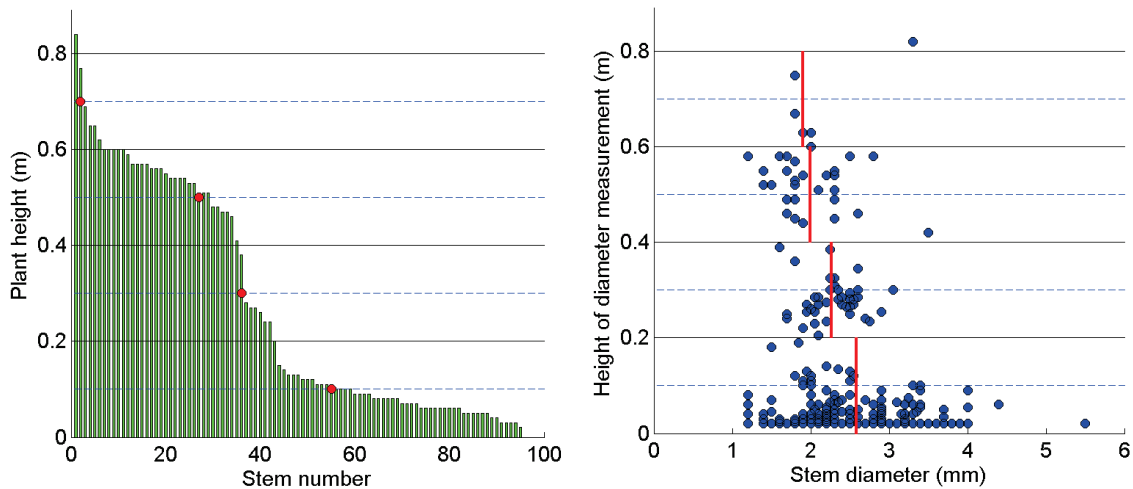


*Figure 8 – Example of the method to determine vegetation characteristics, for Hellegat S3-S4 (Table 3). The stem density in the centre of these layers is equal to 55, 36, 27 and 2 stems per sampled area, or 880, 573, 432 and 30 stems/m2.*

An area of 0.25x0.25 m = 0.0625 m$^2$ was sampled, in which 95 stems were found (Figure 8, left). Four layers have been defined in the SWAN model, with a height of

0.20 m (Hellegat and Bath) or 0.25 m (East Chongming) each. For each stem, the diameter was measured at the base, in the middle, and at the top. Stem diameter and height of the diameter measurement were compared (Figure 8, right). The stem diameter in the four layers of the SWAN model is equal to the mean stem diameter within each layer. The layering was based on the vegetation samples Bath S3-S4 and Hellegat S3-S4. For East Chongming, only one vegetation sample was available. The inter-sample variation in vegetation characteristics was expressed in the model by a spatial varying multiplication factor for the stem density, which was based on the variations in plant surface area $N_v \cdot b_v \cdot h_v$ with respect to sample S3-S4.

*3.2 Model calibration and validation*

As it is expected that wave dissipation by vegetation will prove to be the main dissipation mechanism on vegetated foreshores, the bulk drag coefficient $C_D$ of the Mendez and Losada model in SWAN has been chosen as the main calibration parameter. The wave steepness based formula of Battjes and Stive (1985) has been used to determine suitable breaker parameters $\gamma$ for the Battjes and Janssen (1978) model in SWAN. For bottom friction, the model of Madsen et al. (1988) has been selected, with a constant Nikuradse roughness length scale $k_N = 0.02\,\text{m}$, which is a typical value for a bottom with ripples (Babanin et al., 2005).

For Hellegat and Bath, four tides between 9 Jan 2015, 15:00 and 11 Jan 2015, 9:30 have been selected for the model calibration, and six tides between 20 Dec 2014, 11:30 and 23 Dec 2014, 6:00 for the subsequent model validation. Most tides in the tables with five highest wave heights (Table 4 and Table 5) and inundation depths (Table 6 and Table 7) are included in these two selected periods.

For each burst, a best correspondence between measurement data and outcomes of the SWAN model was obtained, by calibrating the bulk drag coefficient $C_D$. Wave attenuation in most bursts was best reproduced with a value of $C_D$ between 0.2 and 0.9 (Figure 9, left figures), given the method applied to schematize the vegetation with four layers. A decrease in $C_D$ with increasing Re as described in the literature (Table 2) can be recognized. However, there is a considerable spread of drag coefficients around the mean

17

trend, related to many factors that are of influence in the field, such as variations in water depth, wave height and wave period, wave obliqueness, and tidal currents.

Based on the calibration results and the range in Reynolds numbers that apply to the tides in the validation, one characteristic bulk drag coefficient $C_D$ has been selected for each site: 0.5 for Hellegat ($\text{Re} \approx 700$), 0.6 for Bath ($\text{Re} \approx 400$) and 0.4 for East Chongming ($\text{Re} \approx 1200$). These values have been applied to tides outside the calibration period, to guarantee a statistically independent test of the SWAN model. Differences in optimal bulk drag coefficient between the sites are expected to be mainly related to plant stiffness and wave conditions. The validation computations demonstrate that the calibrated SWAN model is able to reproduce the wave height reduction over 50 m of vegetated foreshore with a deviation below 0.05 m (Figure 9, right figures).

At Hellegat, the highest waves in the validation data are present in the tides 54 and 58. At Bath, no inundation of sensor S4 occurred during tide 56. The highest waves and water depths were present during tide 58. At East Chongming, waves and water depths were far higher during tide 10 than during tide 9. For all sites, the SWAN model gives an accurate reproduction of the tides with high waves and water depths, while for tides with lower waves, the wave attenuation is underestimated. Since for each site one constant value of $C_D$ was used for all tides, the observed differences can be explained by the theoretical decline in $C_D$ with $\text{Re}$.
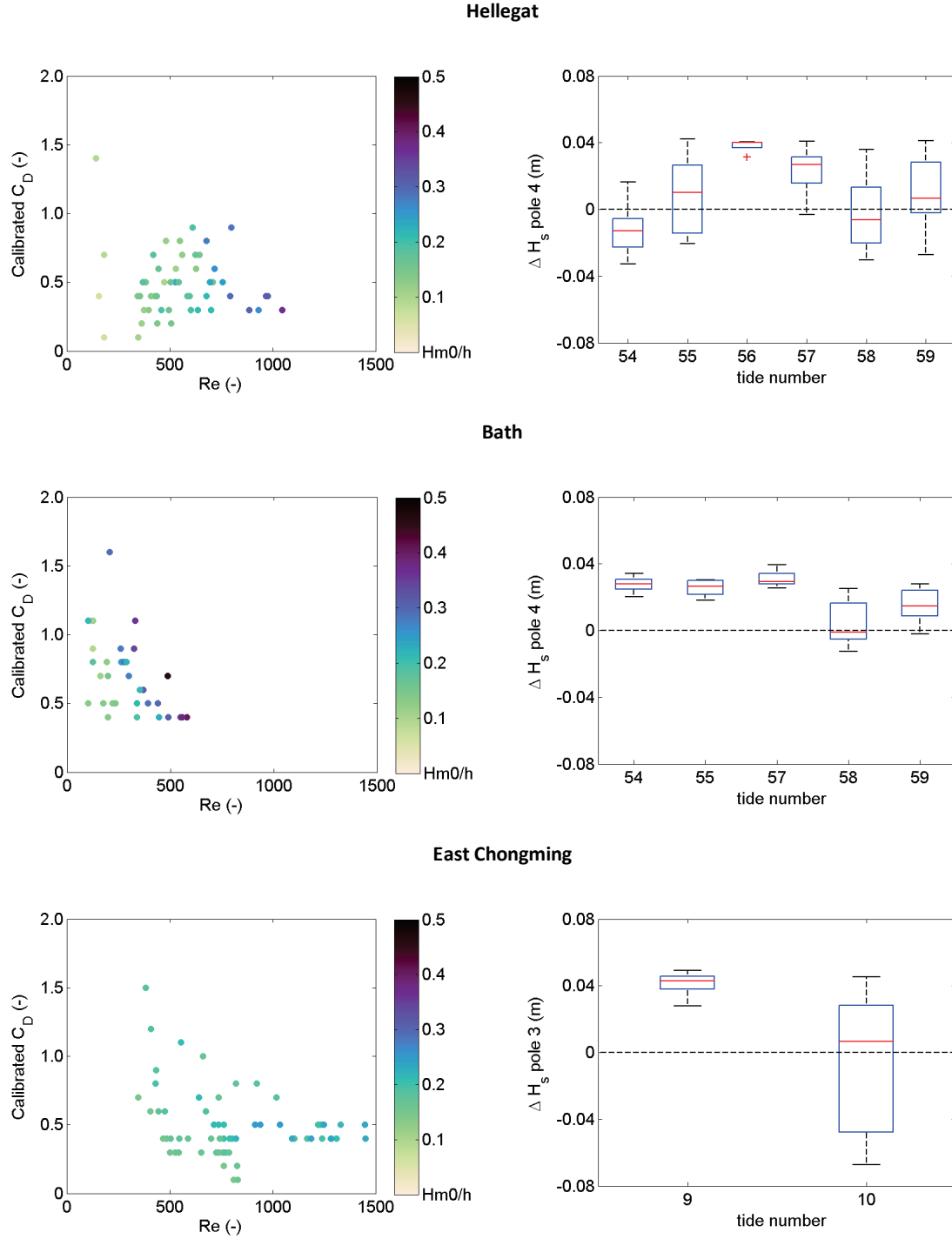
*Figure 9 – Results of the calibration and validation of the SWAN model for the field sites Hellegat (top), Bath (middle) and East Chongming (bottom). For the calibration (figures left), Reynolds numbers are plotted against calibrated drag coefficients for each burst. The markers are coloured by wave height to water depth ratio at sensor S1. For the tides included in the validation (figures right), the differences between modelled and measured significant wave height at sensor S4 are presented. The mean difference (model minus data) is shown in red, the 50 percent interval in blue, and the maximum differences in black.*

### 3.3 Analysis of wave energy dissipation mechanisms

Inclusion of vegetation in the model is essential to reproduce the decay in wave height properly. Wave attenuation by vegetation leads to a gradual decrease in wave height, and prevents intense wave breaking to occur (Figure 10, right panel). In absence of vegetation in the model, waves can retain their energy further inland, and strong wave breaking occurs on the bar in the bottom profile of Hellegat (Figure 10, left panel). Bottom friction is of minor importance for length scales in this order of magnitude. The same processes are present during other tides and at the other sites, Bath and East Chongming.
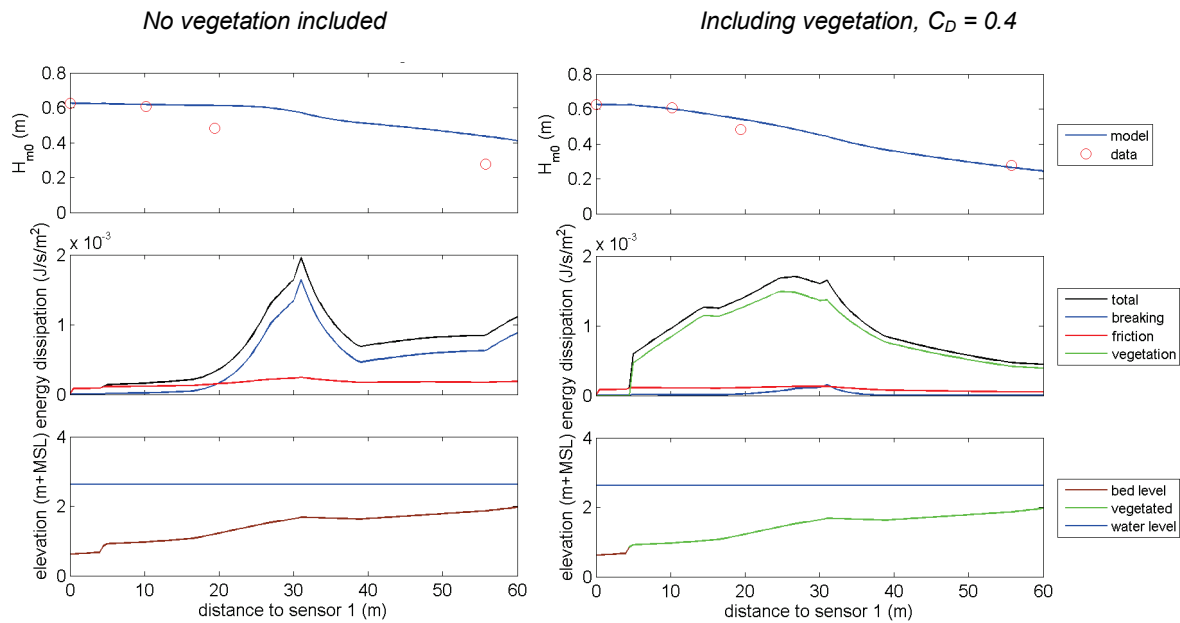


*Figure 10 – Example of reproduction of measured wave heights at Hellegat for one individual burst, for $C_D$ = 0 (no vegetation effect, left) and $C_D$ = 0.4 (right). The upper panels present the observed wave height (red markers) and the model reproduction (blue line) for the bathymetry and water depth shown in the lower panels. The panels in the middle show a comparison of the magnitude of different dissipation mechanisms in the SWAN model.*

If wave energy dissipation by vegetation is excluded in the model, wave heights at sensor S4 are consequently overestimated. The relative importance of vegetation depends on the ratio between wave height and water depth (Figure 11). For very small wave height to water depth ratios at the marsh edge (<0.15), depth-induced wave breaking is negligible and also wave energy dissipation by vegetation is relatively small. For moderate wave height to water depth ratios (0.15-0.30), depth-induced wave breaking on the

foreshore is still limited, but wave attenuation by vegetation can be substantial. The presence of vegetation leads to an additional reduction in significant wave height up to 50% of the total reduction. For larger wave height to water depth ratios at the marsh edge (>0.30), depth-induced wave breaking becomes significant, and the additional contribution of vegetation decreases. However, the model results show that the vegetation dissipates wave energy before intense breaking occurs, since the reduction of wave energy due to the presence of vegetation takes already place at smaller wave height to water depth ratios than the onset of wave breaking (Figure 10). Consequently, the presence of vegetation leads to a more gradual dissipation of wave energy, and a distinct breaker zone is absent. The maximum contribution of vegetation is in the same order of magnitude as the value of 60%, presented in Möller et al. (2014). In their experiments, the contribution of depth-induced wave breaking was relatively low because of the horizontal bottom.
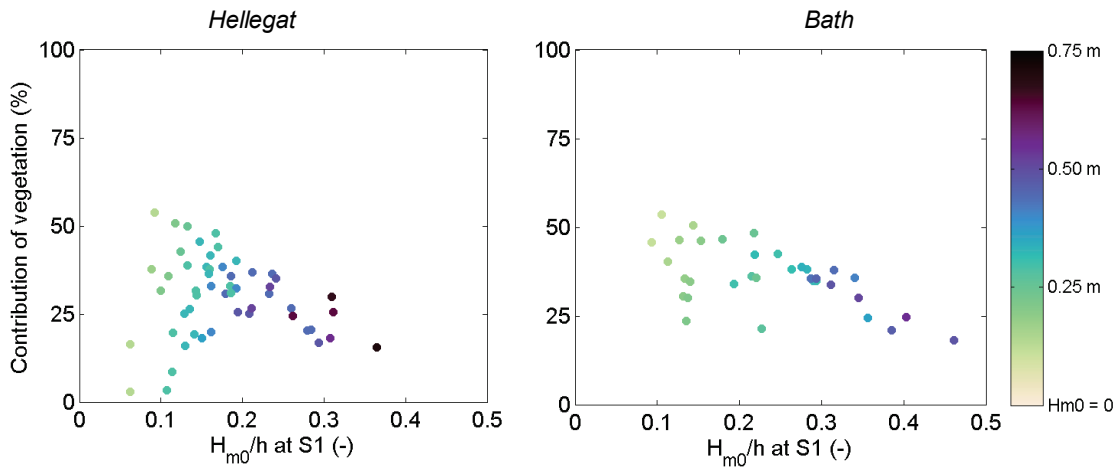


*Figure 11 – Contribution of vegetation (%) to the total reduction in significant wave height between the sensors S1 and S4 at Hellegat (left) and Bath (right), when comparing observed reductions with reductions computed by a SWAN model in which vegetation is excluded. Numbers are given for different wave height to water depth ratios at sensor S1 (horizontal axes), and markers are coloured by wave height at sensor S1.*

## 4  Wave load reduction by vegetated foreshores

The previous sections have demonstrated the wave damping capacity of vegetated foreshores. Since wave overtopping over the dike is strongly related to the incident wave height, wave energy dissipation by vegetated foreshores allows in principle for lower crest heights, and consequently, relatively slender dike bodies. This section shows some examples of the effect of vegetated foreshores on wave loads on coastal dikes for a range of foreshore configurations and hydraulic loading conditions.

## 4.1 Approach

The wave transformation over the vegetated foreshore is estimated by applying the validated SWAN model (section 3). The formulas presented in EurOtop (2007) are used to calculate the characteristic two percent wave run-up height on the outer slope of the dike (formula 5.3) and the time-averaged wave overtopping discharge over the dike (formulas 5.8 and 5.11). Wave conditions at the toe of the dike should be supplied to these formulas. The validated SWAN model is used to compute wave height reduction over vegetated foreshores for various foreshore configurations and hydraulic loading conditions (Figure 12), including the influence of the vegetated foreshore on the wave conditions as computed by SWAN. Because of the complex and context-dependent influence of vegetated foreshores on storm surge propagation (Wamsley et al., 2010; Zhang et al., 2012) and wave set-up (Battjes, 1974; Dean and Bender, 2006), we ignore these effects in the present study.
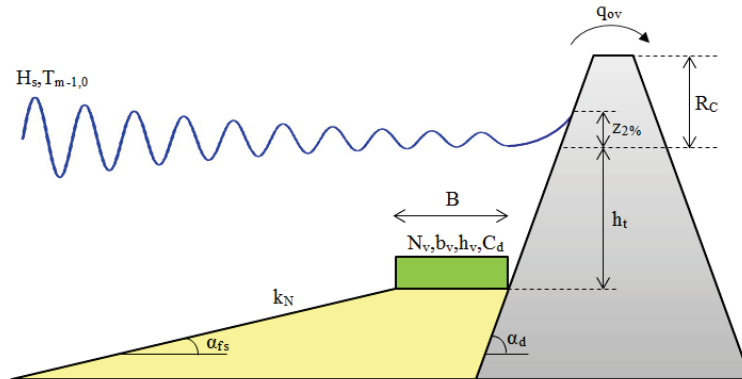


Figure 12 – Definition sketch of a schematized dike-foreshore system. Table 8 gives an overview of the variables involved.

In the Netherlands, salt marshes are generally enclosed by a dike at the landward side, and an adjacent mudflat in front. The slope of these combined salt marsh-mudflat systems depends on the available space. For example in the Western Scheldt estuary, lateral dimensions of salt marshes similar to Hellegatpolder (Figure 1, upper right) are limited by the presence of deep tidal channels, intensively used for navigation. At the salt marshes bordering the Wadden Sea in the north of the Netherlands, a smooth transition between the salt marshes and the extensive intertidal flats is often present. This is for example the case at the salt marshes near Groningen and Texel (Figure 1, lower left and

right). Sandy foreshores with relatively steep slopes (about 1:50) can be found in front of dikes directly bordering the North Sea, for example at the Westkapelle sea defence (Figure 1, upper left). The hydrodynamic forcing at these foreshores is generally too intense to allow vegetation seedlings to settle.

Inundation depths depend on the salt marsh elevation and storm surge levels. The maximum elevation of the marshes is strongly related to the local tidal amplitude. Surge levels depend on tidal amplitude and surge effects. Under design conditions in the Netherlands, inundation depths above salt marsh surface can typically reach values between 1.5 and 3.5 m near the dike toe. Depending on the location and orientation of the dike with respect to the prevailing wind direction during storms, incident wave heights vary roughly between 0.5 and 2.0 m. Salt marshes do generally not develop in areas that are exposed to even more energetic conditions. To achieve stable dike slope revetments, designers can opt for relatively steep slopes, typically around 1:3, combined with heavy armouring units. More gentle slopes, in the order of 1:6, allow for the use of lighter revetments. Depending on incident wave conditions, the relative freeboard is mostly in the range of 2.5 to 4.5 m.

Based on these different examples of salt marshes in the Netherlands, characteristic vegetated foreshore characteristics are defined (Table 8), with variation in water depth, foreshore width and vegetation coverage (no vegetation or vegetation resembling *Spartina anglica* in winter state). Based on the calibration results (Figure 9), a bulk drag coefficient of 0.4 is considered as an initial estimate for salt marsh vegetation at large Reynolds numbers.

23

*Table 8 – Definition of variables used to schematize the characteristics of the dike-foreshore system (Figure 12) and the hydrodynamic loads on the system.*

| Parameter | | Name | Units | Values |
|---|---|---|---|---|
| 1 | $\alpha_d$ | Slope angle dike | - | 1:4 |
| 2 | $R_c$ | Relative freeboard | m | 3.0 |
| 2 | $\alpha_{fs}$ | Slope angle tidal flat | - | 1:100 |
| 3 | $h_t$ | Water depth at dike toe | m | 1.0-4.0 |
| 4 | $H_{m0}$ | Offshore significant wave height | m | 1.5 |
| 5 | $T_{m-1,0}$ | Offshore spectral wave period | s | 5.0 |
| 6 | $k_N$ | Roughness length scale | m | 0.02 |
| 7 | B | Width of flat part of foreshore | m | 0-800 |
| 8 | $N_v$ | Stem density | stems/m$^2$ | 0, 1200 |
| 9 | $b_v$ | Stem diameter | mm | 3.0 |
| 10 | $h_v$ | Vegetation height | m | 0.30 |
| 11 | $C_d$ | Bulk drag coefficient vegetation | - | 0.4 |
| 12 | $z_{2\%}$ | Two percent wave run-up height | m | - |
| 13 | $q_{ov}$ | Mean overtopping discharge | m$^3$s$^{-1}$m$^{-1}$ | - |

## 4.2 Computational results

For the dike configuration and wave characteristics of Table 8, a two percent wave run-up height $z_{2\%}$ of approximately 3.2 m will occur without any disturbance of the waves on a foreshore. Because the relative freeboard in this case study is only 3.0 m, this would result in a mean overtopping discharge of 0.6 l s$^{-1}$ m$^{-1}$. Figure 13 shows the relative reduction of significant wave height (top panel), wave run-up height (middle panel) and reduction factor in wave overtopping discharge (bottom panel) due to the presence of bare foreshores (left panels) and vegetated foreshores (right panels), depending on foreshore width (horizontal axis) and depth on the foreshore (vertical axis).

If the depth on the foreshore is limited to just 1.0 m, the wave run-up is reduced by 60-100%, and the wave overtopping discharge diminishes to negligible amounts. For larger water depths, the influence of vegetation becomes more distinct. In the Netherlands, typical design water levels are in the order of 5 m above mean sea level, which is 3 m above the salt marsh surface. Where wave run-up under these conditions is only reduced by approximately 20% (0.6 m) for a 400 m wide, bare foreshore, the same foreshore covered by vegetation resembling *Spartina anglica* in winter state reduces the wave run-up by 55% (1.8 m). Wave overtopping discharges still have significant values for bare foreshores in case of large water depths, whereas the presence of vegetation fully prevents the occurrence of overtopping.

**Reduction in significant wave height (%)**



**Reduction in 2 percent wave run-up height (%)**



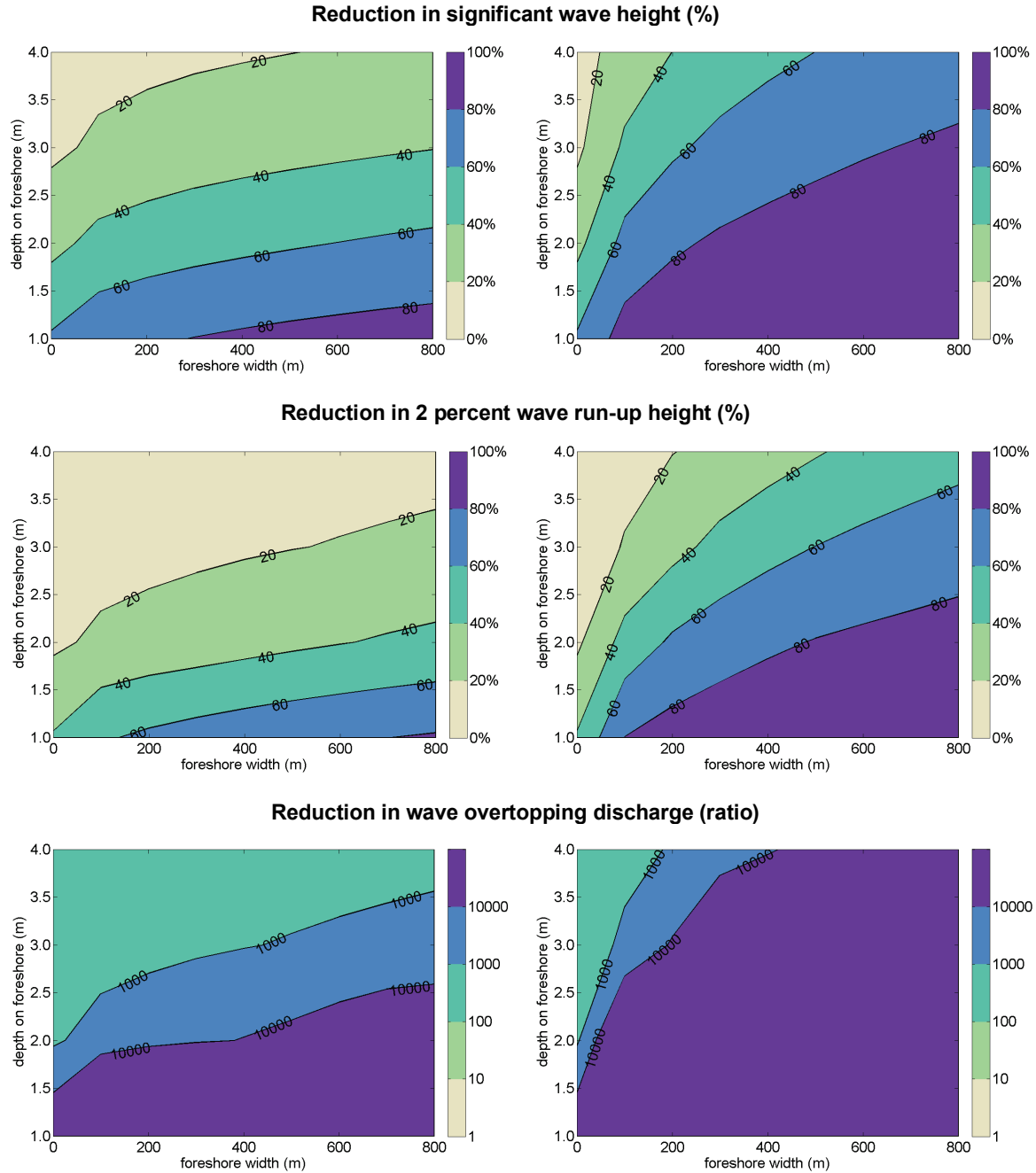**Reduction in wave overtopping discharge (ratio)**



*Figure 13 – Relative reduction in significant wave height (top), 2 percent wave run-up height (middle) and reduction factor in wave overtopping discharge (bottom), in case of bare foreshores (left panels) and vegetated foreshores (right panels), for the values in Table 8.*

Some trends can be discerned. For foreshores with a small width, depth-induced wave breaking dominates the total wave energy dissipation. Bottom friction and wave attenuation by vegetation gain relative importance with increasing width. The dependence of wave load reduction with depth is non-linear, which is caused by the onset of wave

25

breaking at a certain depth. For larger depths, the relative importance of vegetation increases, since wave energy dissipation by vegetation already acts at lower wave height to water depth ratios than depth-induced wave breaking (Figure 11). The relationship with foreshore width is non-linear as well, because of the dependence of wave energy dissipation on wave height.

The required crest height of a coastal dike is strongly related to the wave run-up height under design conditions. Because of the non-linear relation between wave run-up and wave height, the effect of foreshores on the wave run-up height is lower than their effect on the incident wave height. This difference is essential when interpreting wave attenuation by vegetation and foreshores. Mostly, dikes are designed in such a way that the wave overtopping discharge is limited to a tolerable rate under design conditions. Because of the exponential relation between overtopping discharge and wave height (EurOtop, 2007), the presence of a vegetated foreshore might make the difference between a significant overtopping discharge and full absence of overtopping. The results of these explorative computations highlight the demand for integrating foreshore dimensions as well as vegetation characteristics in the design and assessment of coastal dikes.

## 5  Discussion

This paper presents a combination of a literature review, field measurements and numerical modelling of wave attenuation by vegetation under storm conditions. The numerical model has been applied to assess the efficiency of vegetated foreshores in reducing wave loads on coastal dikes under design conditions. In this section, the field measurements and numerical modelling work is discussed. Additionally, attention is payed to the applicability of the results and demands for further research.

### 5.1 Field measurements

The field measurements of wave attenuation by vegetation, as described in this paper, have added to the highest range of wave heights and water depths, as currently available in the literature. These new measurements reduce the gap between measured conditions and design conditions for the flood defences. The current study is based on measurements of wave attenuation over salt marshes, in combination with computed wave run-up and wave overtopping. Quantification of the effect of vegetated foreshores

can be improved when measurements of wave attenuation by vegetation are accompanied by measurements of wave run-up heights and wave overtopping discharges.

## 5.2 Model used

To compute wave loads on coastal dikes with vegetated foreshore in front, a combination of SWAN for the wave transformation over the vegetated foreshore and analytical formulas for wave run-up and wave overtopping has been applied. Both components of this approach limit the applicability of the results to a certain range. SWAN is not able to compute the generation and propagation of infragravity waves, since it is a spectral domain model. At the salt marshes that were included in the calibration study of this paper, the fraction of wave energy captured in long waves was very limited (less than 1% during storms). Application of the results of this study is restricted to situations where the wave regime is characterized by local wind sea and swell waves, and the presence of infragravity waves should be of minor importance for the wave loads on the dike. This is the case in many estuaries and coastal seas, where salt marshes are found. If significant infragravity wave energy is to be expected, it is better to use another numerical model, such as SWASH (Zijlema et al., 2011) or XBeach (Roelvink et al., 2009).

The SWAN model contains approximations for wave energy dissipation by bottom friction and due to vegetation. Both dissipation models are based on linear wave theory, under the assumption of orbital velocity profiles according to linear wave theory. However, bottom friction affects near-bottom orbital velocities, and the presence of vegetation reduces orbital velocities in the submerged canopy. Consequently, the dissipation rates by both mechanisms are interdependent in reality. Higher bottom friction leads to lower dissipation due to vegetation and vice versa. In the SWAN model, their contributions are computed separately and added to the total wave energy dissipation. This methodologic error influences model results such as the computed dissipation rates by both mechanisms and the bulk drag coefficient $C_D$ that follows by calibration.

The modelled rate of wave attenuation by vegetation strongly depends on the imposed bulk drag coefficient. In the calibration of the numerical model, a considerable variation in the calibrated drag coefficient was found. Many authors attempt to describe the drag coefficient as a function of the vegetation Reynolds number or the Keulegan Carpenter number. In both quantities, the stem diameter is used as characteristic length scale.

27

Differences in stem diameter is one of the main reasons for the large variation between the expressions that are proposed in the literature (Table 2). It is questionable whether such calibrated relations can be applied to vegetation types with significantly other characteristics such as stem diameter and flexibility. Studies that help to explain the physics behind the observed variation in vegetation drag coefficients can be useful in this context.

## 5.3 Morphological stability

The wave load reduction by vegetated foreshores relies on the stability of both bathymetry and vegetation. The bottom surface of salt marshes consists of consolidated clay and root systems. For such bottoms, significant surface erosion during storms is not to be expected. This is in agreement with post-storm observation (Dijkema et al., 2011; Spencer et al., 2015), large-scale wave flume experiments (Möller et al., 2014) and process descriptions (Winterwerp et al., 2012). The present study shows an additional reason for the stable character of salt marsh sediments. The presence of vegetation prevents intense wave breaking to occur, since the wave energy is dissipated more gradually by the vegetation. As wave breaking can lead to high sediment pick-up rates and severe erosion, this means that vegetation enhances the stable character of the salt marsh surface.

## 5.4 Reliability of dike-foreshore systems

Before nature-based flood defences can be considered as full alternatives for conventional flood defences, they need to be tested according to engineering standards for probability of failure (Van Wesenbeeck et al., 2014). The probability of failure of a flood defence is defined as the probability that the flood defence fails in fulfilling its function: the protection of social and economic value against flooding. To be able to assess the actual reliability of dike-foreshore systems in terms of a probability of failure, quantification of knowledge uncertainties as well as inherent uncertainties is required, see e.g. Vrijling (2001). The uncertainty in the choice of a suitable vegetation drag coefficient is one of the main knowledge uncertainties involved. This type of uncertainty is distinct from inherent uncertainty, which is related to the natural randomness in samples (Van Gelder, 2000). Examples of the latter include spatial and seasonal variations in vegetation properties. This study is part of the research programme BE SAFE. Further research

in this project should lead to more insights in the uncertainties regarding wave attenuation by vegetated foreshores.

## 5.5  Implications for management

This study shows that vegetated foreshores with a width of several tens of metres can reduce wave loads on coastal dikes during severe storm significantly. Therefore, dike managers may consider construction or maintenance of vegetated foreshores as a serious supplement to the possibilities for traditional dike reinforcement such as raising the dike crest or strengthening the inner or outer slope revetment. In many deltas, vegetated foreshores such as salt marshes and reed fields are already present along the dikes. In that case, it is probably worth considering to take their influence on wave loads into account in flood risk assessments. Once the foreshores are formally part of the flood defence, the challenge shifts from the design of an appropriate foreshore to the establishment of assessment protocols and institutional arrangements for monitoring and management. The usage of a foreshore as a dike reinforcement strategy might be particularly attractive when a shallow foreshore is already present, or when site-specific conditions impede traditional reinforcements methods.

## 6  Conclusions

Application of vegetated foreshores has been increasingly mentioned as an effective method to reduce wave heights that act on coastal dikes. However, the efficiency of vegetated foreshores in reducing wave energy under severe storm conditions with high waves and large water depths is not well understood. Most existing empirical studies only quantify wave attenuation for moderate wave conditions in combination with limited water depths. The wave measurements described in this study have added to the range of observations with the highest water depths (up to 2.5 m) and wave heights (up to 0.7 m) presented in the literature so far. The measurements were performed on two salt marshes with two representative but contrasting coastal wetland vegetation types: cordgrass (*Spartina anglica*) and grassweed (*Scirpus maritimus*). The former is found in salty environments, whereas the latter is found in brackish environments. The measurements shed light on wave attenuation by vegetation under severe storm conditions, and have successfully been used to calibrate and validate the numerical model SWAN that describes wave propagation over vegetated foreshores. It appeared that the observed

wave attenuation by vegetation under storm conditions could best be described by a bulk drag coefficient $C_D \approx 0.4$.

Vegetated foreshores can reduce wave energy during severe storm conditions significantly. Even though energy dissipation by vegetation is most effective at small water depths and with high biomass, the wave energy reduction for larger inundation depths and the vegetation being in winter state is still considerable. Vegetation drag substantially contributes to the total wave energy dissipation. The presence of vegetation leads to an additional reduction rate of the significant wave height of 25-50% with respect to the dissipation by only wave breaking and bottom friction on the sloping transects. Under storm conditions with relatively small wave height to water depth ratios, depth-induced wave breaking on the foreshore is limited, but wave attenuation by vegetation can already be substantial. For larger wave height to water depth ratios, the presence of vegetation prevents intense wave breaking to occur, since the wave energy is dissipated more gradually. The absence of intense wave breaking might contribute to the stable character of the salt marsh sediments.

The calibrated and validated SWAN model has been applied to compute wave height reduction over vegetated foreshores for various foreshore configurations and hydraulic loading conditions. The computed wave conditions at the toe of the dike have been used to determine the efficiency of vegetated foreshores in reducing the wave run-up height on the outer slope of the dike and the wave overtopping discharge over the dike. Both bare foreshores and vegetated foreshores can lead to a major decrease in wave run-up height and wave overtopping discharge when the water depth on the foreshore can be reduced to one or two times the significant wave height. However, when vegetation is present under these conditions, the main dissipation mechanism shifts from intense wave breaking to more gradual dissipation of wave energy due to the vegetation. For larger depths, the relative importance of vegetation increases, since wave energy dissipation by vegetation already acts at lower wave height to water depth ratios than depth-induced wave breaking. This means that vegetation extends the range of water depths for which a foreshore can be applied for effective reduction of wave loads. Bottom friction as well as wave attenuation by vegetation gain relative importance with increasing foreshore width. Since foreshores have a significant effect on wave run-up and overtopping,

it is desirable to include the foreshore characteristics in the design and assessment of coastal dikes.

The reduction in wave loads that follows from observations in the field and computations with a calibrated numerical model shows that vegetated foreshores can be considered as a valuable supplement to conventional engineering methods for dike reinforcement.

## References

Allen, J.H., Nuechterlein, G.L., Buitron, D. (2008). Bulrush Mediation Effects on Wave Action: Implications for Over-water Nesting Birds, *31*, 411–416.

Anderson, M.E., Smith, J.M. (2014). Wave attenuation by flexible, idealized salt marsh vegetation. *Coastal Engineering*, *83*, 82–92.

Anderson, M.E., Smith, J.M., McKay, S.K. (2011). *Wave dissipation by vegetation*. US Army Engineer Research and Development Center.

Arkema, K.K., Guannel, G., Verutes, G., Wood, S.A., Guerry, A., Ruckelshaus, M., Kareiva, P., Lacayo, M., Silver, J.M. (2013). Coastal habitats shield people and property from sea-level rise and storms. *Nature Climate Change*, *3*, 913–918.

Asano, T., Deguchi, H., Kobayashi, N. (1992). Interaction between water waves and vegetation. *Coastal Engineering Proceedings*, *1*.

Augustin, L.N., Irish, J.L., Lynett, P. (2009). Laboratory and numerical studies of wave damping by emergent and near-emergent wetland vegetation. *Coastal Engineering*, *56*, 332–340.

Babanin, A. V, Young, I., Mirfenderesk, H. (2005). Field and laboratory measurements of wave-bottom interaction.

Battjes, J.A. (1974). *Computation of set-up, longshore currents, run-up and overtopping due to wind-generated waves*. Department of Civil Engineering, Delft University of Technology.

Battjes, J.A., Janssen, J.P.F.M. (1978). Energy loss and set-up due to breaking of random waves. *Coastal Engineering Proceedings*.

Battjes, J.A., Stive, M.J.F. (1985). Calibration and verification of a dissipation model for random breaking waves. *Journal of Geophysical Research: …*, 649–660.

Booij, N., Ris, R.C., Holthuijsen, L.H. (1999). A third-generation wave model for coastal regions: 1. Model description and validation. *Journal of Geophysical Research*, *104*, 7649.

Borsje, B.W., van Wesenbeeck, B.K., Dekker, F., Paalvast, P., Bouma, T.J., van Katwijk, M.M., de Vries, M.B. (2011). How ecological engineering can serve in coastal protection. *Ecological Engineering*, *37*, 113–122.

Bouma, T.J., De Vries, M.B., Low, E., Peralta, G., Tánczos, I.C., van de Koppel, J., Herman, P.M.J. (2005). Trade-Offs Related To Ecosystem Engineering: a Case Study on Stiffness of Emerging Macrophytes. *Ecology*, *86*, 2187–2199.

Bouma, T.J., van Belzen, J., Balke, T., Zhu, Z., Airoldi, L., Blight, A.J., Davies, A.J., Galvan, C., Hawkins, S.J., Hoggart, S.P.G., Lara, J.L., Losada, I.J., Maza, M., Ondiviela, B., Skov, M.W., Strain, E.M., Thompson, R.C., Yang, S., Zanuttigh, B., Zhang, L., Herman, P.M.J. (2014). Identifying knowledge gaps hampering application of intertidal habitats in coastal protection: Opportunities & steps to take. *Coastal Engineering*, *87*, 147–157.

Bradley, K., Houser, C. (2009). Relative velocity of seagrass blades : Implications for wave attenuation in low-energy environments, *114*, 1–13.

Cooper, N. (2005). Wave dissipation across intertidal surfaces in the Wash Tidal Inlet, Eastern England. *Journal of Coastal Research*, 28–40.

Coops, H., Geilen, N., Verheij, H.J., Boeters, R., van der Velde, G. (1996). Interactions between waves, bank erosion and emergent vegetation: an experimental study in a wave tank. *Aquatic Botany*, *53*, 187–198.

Dalrymple, R.A., Kirby, J.T., Hwang, P.A. (1984). Wave diffraction due to areas of energy dissipation. *Journal of Waterway, Port, Coastal, and Ocean Engineering*, *110*, 67–79.

Dean, R.G., Bender, C.J. (2006). Static wave setup with emphasis on damping effects by vegetation and bottom friction. *Coastal Engineering*, *53*, 149–156.

Dijkema, K.S., Van Duin, W.E., Dijkman, E.M., Nicolai, E., Jongerius, H., Keegstra, H., Van Egmond, L., Venema, H.J., Jongsma, J.J. (2011). *Vijftig jaar monitoring en beheer van de Friese en Groninger kwelderwerken: 1960-2009*. Wageningen UR, Wageningen.

Dijkstra, J.T., Uittenbogaard, R.E. (2010). Modeling the interaction between flow and highly flexible aquatic vegetation. *Water Resources Research*, *46*, 1–14.

Dubi, A., Torum, A. (1996). Wave energy dissipation in kelp vegetation. *Coastal Engineering Proceedings*, 2626–2639.

Duncan, J.H. (1983). The breaking and non-breaking wave resistance of a two-dimensional hydrofoil.

*Journal of Fluid Mechanics*, *126*, 507–520.

EurOtop. (2007). *Wave overtopping of sea defences and related structures: assessment manual*. (T. Pullen, N. W. H. Allsop, T. Bruce, A. Kortenhaus, H. Schüttrumpf, & J. W. Van der Meer, Eds.).

Fonseca, M., Cahalan, J. (1992). A preliminary evaluation of wave attenuation by four species of seagrass. *Estuarine, Coastal and Shelf Science*, 565–576.

Gedan, K.B., Kirwan, M.L., Wolanski, E., Barbier, E.B., Silliman, B.R. (2010). The present and future role of coastal wetland vegetation in protecting shorelines: answering recent challenges to the paradigm. *Climatic Change*, *106*, 7–29.

Horstman, E.M., Dohmen-Janssen, C.M., Narra, P.M.F., van den Berg, N.J.F., Siemerink, M., Hulscher, S.J.M.H. (2014). Wave attenuation in mangroves: A quantitative approach to field observations. *Coastal Engineering*, *94*, 47–62.

Hu, Z., Suzuki, T., Zitman, T., Uittewaal, W., Stive, M. (2014). Laboratory study on wave dissipation by vegetation in combined current-wave flow. *Coastal Engineering*, *88*, 131–142.

Jadhav, R., Chen, Q. (2012). Field investigation of wave dissipation over salt marsh vegetation during tropical cyclone. *Coastal Engineering Proceedings*, *1*, 1–11.

Jadhav, R.S., Chen, Q., Smith, J.M. (2013). Spectral distribution of wave energy dissipation by salt marsh vegetation. *Coastal Engineering*, *77*, 99–107.

Jones, H.P., Hole, D.G., Zavaleta, E.S. (2012). Harnessing nature to help people adapt to climate change. *Nature Climate Change*, *2*, 504–509.

King, S.E., Lester, J.N. (1995). The Value of Salt Marsh as a Sea Defence. *Marine Pollution Bulletin*, *30*, 180–189.

Knutson, P., Brochu, R., Seelig, W., Inskeep, M. (1982). Wave damping in Spartina alterniflora marshes. *Wetlands*, 87–104.

Kobayashi, N., Raichle, A.W., Asano, T. (1993). Wave Attenuation by Vegetation. *Journal of Waterway, Port, Coastal, and Ocean Engineering*, *119*, 30–48.

Koftis, T., Prinos, P., Stratigaki, V. (2013). Wave damping over artificial Posidonia oceanica meadow: A large-scale experimental study. *Coastal Engineering*, *73*, 71–83.

Liffen, T., Gurnell, a. M., O'Hare, M.T., Pollen-Bankhead, N., Simon, a. (2013). Associations between the morphology and biomechanical properties of Sparganium erectum: Implications for survival and ecosystem engineering. *Aquatic Botany*, *105*, 18–24.

Madsen, O., Poon, Y., Graber, H. (1988). Spectral Wave Attenuation by Bottom Friction: Theory. *Proceedings of the 21th Int. Conf. Coastal Engineering*, 492–504.

Manca, E., Cáceres, I., Alsina, J.M., Stratigaki, V., Townend, I., Amos, C.L. (2012). Wave energy and wave-induced flow reduction by full-scale model Posidonia oceanica seagrass. *Continental Shelf Research*, *50-51*, 100–116.

Massel, S. (1996). On the largest wave height in water of constant depth. *Ocean Engineering*, *23*, 553–573.

Mazda, Y., Magi, M., Ikeda, Y., Kurokawa, T., Asano, T. (2006). Wave reduction in a mangrove forest dominated by Sonneratia sp. *Wetlands Ecology and Management*, *14*, 365–378.

Mei, C.C., Chan, I.-C., Liu, P.L.-F., Huang, Z., Zhang, W. (2011). Long waves through emergent coastal vegetation. *Journal of Fluid Mechanics*, *687*, 461–491.

Mendez, F.J., Losada, I.J. (2004). An empirical model to estimate the propagation of random breaking and nonbreaking waves over vegetation fields. *Coastal Engineering*, *51*, 103–118.

Méndez, F.J., Losada, I.J., Losada, M.A. (1999). Hydrodynamics induced by wind waves in a vegetation field. *Journal of Geophysical Research: Oceans (1978--2012)*, *104*, 18383–18396.

Möller, I. (2006). Quantifying saltmarsh vegetation and its effect on wave height dissipation: Results from a UK East coast saltmarsh. *Estuarine, Coastal and Shelf Science*, *69*, 337–351.

Möller, I., Kudella, M., Rupprecht, F., Spencer, T., Paul, M., van Wesenbeeck, B.K., Wolters, G., Jensen, K., Bouma, T.J., Miranda-Lange, M., Schimmels, S. (2014). Wave attenuation over coastal salt marshes under storm surge conditions. *Nature Geoscience*, *7*, 727–731.

Möller, I., Mantilla-Contreras, J., Spencer, T., Hayes, a. (2011). Micro-tidal coastal reed beds: Hydro-morphological insights and observations on wave transformation from the southern Baltic Sea. *Estuarine, Coastal and Shelf Science*, *92*, 424–436.

Möller, I., Spencer, T. (2002). Wave dissipation over macro-tidal saltmarshes: Effects of marsh edge typology and vegetation change. *Journal of Coastal Research*, *521*, 506–521.

Möller, I., Spencer, T., French, J.R., Leggett, D.J., Dixon, M. (1999). Wave Transformation Over Salt Marshes: A Field and Numerical Modelling Study from North Norfolk, England. *Estuarine, Coastal and Shelf Science*, *49*, 411–426.

Mullarney, J.C., Henderson, S.M. (2010). Wave-forced motion of submerged single-stem vegetation. *Journal of Geophysical Research*, *115*, C12061.

Nairn, R.B. (1990). *Prediction of cross-shore sediment transport and beach profile evolution.* Imperial College London (University of London).

Nelson, R.C. (1994). Depth limited design wave heights in very flat regions. *Coastal Engineering*, *23*, 43–59.

Padilla-Hernández, R., Monbaliu, J. (2001). Energy balance of wind waves as a function of the bottom friction formulation. *Coastal Engineering*, *43*, 131–148.

Paul, M., Amos, C.L. (2011). Spatial and seasonal variation in wave attenuation over Zostera noltii. *Journal of Geophysical Research: Oceans*, *116*, 1–16.

Pinsky, M., Guannel, G., Arkema, K. (2013). Quantifying wave attenuation to inform coastal habitat conservation. *Ecosphere*, *4*.

Puijalon, S., Bouma, T.J., Douady, C.J., van Groenendael, J., Anten, N.P.R., Martel, E., Bornette, G. (2011). Plant resistance to mechanical stress: evidence of an avoidance-tolerance trade-off. *The New*

*Phytologist*, *191*, 1141–9.

Pujol, D., Serra, T., Colomer, J., Casamitjana, X. (2013). Flow structure in canopy models dominated by progressive waves. *Journal of Hydrology*, *486*, 281–292.

Quartel, S., Kroon,  a., Augustinus, P.G.E.F., Van Santen, P., Tri, N.H. (2007). Wave attenuation in coastal mangroves in the Red River Delta, Vietnam. *Journal of Asian Earth Sciences*, *29*, 576–584.

Riffe, K.C., Henderson, S.M., Mullarney, J.C. (2011). Wave dissipation by flexible vegetation. *Geophysical Research Letters*, *38*.

Ris, R.C., Holthuijsen, L.H., Booij, N. (1999). A third-generation wave model for coastal regions: 2. Verification. *Journal of Geophysical Research*, *104*, 7667.

Roelvink, D., Reniers, A., van Dongeren, A., van Thiel de Vries, J., McCall, R., Lescinski, J. (2009). Modelling storm impacts on beaches, dunes and barrier islands. *Coastal Engineering*, *56*, 1133–1152.

Ruessink, B.G., Walstra, D.J.R., Southgate, H.N. (2003). Calibration and verification of a parametric wave model on barred beaches. *Coastal Engineering*, *48*, 139–149.

Rupprecht, F., Möller, I., Evans, B., Spencer, T., Jensen, K. (2015). Biophysical properties of salt marsh canopies — Quantifying plant stem flexibility and above ground biomass. *Coastal Engineering*, *100*, 48–57.

Sánchez-González, J.F., Sánchez-Rojas, V., Memos, C.D. (2011). Wave attenuation due to Posidonia oceanica meadows. *Journal of Hydraulic Research*, *49*, 503–514.

Seymour, R., Tegner, M. (1989). Storm wave induced mortality of giant kelp, Macrocystis pyrifera, in Southern California. *Estuarine, Coastal and Shelf Science*, *28*, 277–292.

Spencer, T., Brooks, S.M., Evans, B.R., Tempest, J.A., Möller, I. (2015). Southern North Sea storm surge event of 5 December 2013: Water levels , waves and coastal impacts. *Earth-Science Reviews*, *146*, 120–145.

Stratigaki, V., Manca, E., Prinos, P., Losada, I.J., Lara, J.L., Sclavo, M., Amos, C.L., Cáceres, I., Sánchez-Arcilla, A. (2011). Large-scale experiments on wave propagation over Posidonia oceanica. *Journal of Hydraulic Research*, *49*, 31–43.

Sutton-Grier, A.E., Wowk, K., Bamford, H. (2015). Future of our coasts: the potential for natural and hybrid infrastructure to enhance the resilience of our coastal communities, economies and ecosystems. *Environmental Science and Policy*, *51*, 137–148.

Suzuki, T. (2011). *Wave dissipation over vegetation fields*. Delft University of Technology, Delft.

Suzuki, T., Arikawa, T. (2011). Numerical analysis of bulk drag coefficient in dense vegetation by immersed boundary method. In *Coastal Engineering Proceedings*.

Suzuki, T., Zijlema, M., Burger, B., Meijer, M.C., Narayan, S. (2012). Wave dissipation by vegetation with layer schematization in SWAN. *Coastal Engineering*, *59*, 64–71.

Temmerman, S., Meire, P., Bouma, T.J., Herman, P.M.J., Ysebaert, T., De Vriend, H.J. (2013). Ecosystem-

based coastal defence in the face of global change. *Nature*, *504*, 79–83.

Van Gelder, P.H.A.J.M. (2000). *Statistical methods for the risk-based design of civil structures*. TU Delft, Delft University of Technology.

Van Gent, M.R.A., Doorn, N. (2001). Numerical model simulations of wave propagation and wave run-up on dikes with shallow foreshores. In *Proc. of 4th Coastal Dynamics Conference* (pp. 769–778).

Van Wesenbeeck, B.K., Mulder, J.P.M., Marchand, M., Reed, D.J., de Vries, M.B., de Vriend, H.J., Herman, P.M.J. (2014). Damming deltas: A practice of the past? Towards nature-based flood defenses. *Estuarine, Coastal and Shelf Science*, *140*, 1–6.

Vrijling, J.K. (2001). Probabilistic design of water defense systems in The Netherlands. *Reliability Engineering & System Safety*, *74*, 337–344.

Wamsley, T. V., Cialone, M. a., Smith, J.M., Atkinson, J.H., Rosati, J.D. (2010). The potential of wetlands in reducing storm surge. *Ocean Engineering*, *37*, 59–68.

Weber, S.L. (1989). *Surface gravity waves and turbulent bottom friction*. University of Utrecht, The Netherlands.

Winterwerp, J.C., van Kesteren, W.G.M., van Prooijen, B., Jacobs, W. (2012). A conceptual framework for shear flow–induced erosion of soft cohesive sediment beds. *Journal of Geophysical Research*, *117*, C10020.

Yang, S.L., Shi, B.W., Bouma, T.J., Ysebaert, T., Luo, X.X. (2012). Wave Attenuation at a Salt Marsh Margin: A Case Study of an Exposed Coast on the Yangtze Estuary. *Estuaries and Coasts*, *35*, 169–182.

Ysebaert, T., Yang, S.-L., Zhang, L., He, Q., Bouma, T.J., Herman, P.M.J. (2011). Wave Attenuation by Two Contrasting Ecosystem Engineering Salt Marsh Macrophytes in the Intertidal Pioneer Zone. *Wetlands*, *31*, 1043–1054.

Zhang, K., Liu, H., Li, Y., Xu, H., Shen, J., Rhome, J., Smith, T.J. (2012). The role of mangroves in attenuating storm surges. *Estuarine, Coastal and Shelf Science*, *102-103*, 11–23.

Zijlema, M., Stelling, G., Smit, P. (2011). SWASH: An operational public domain code for simulating wave fields and rapidly varied flows in coastal waters. *Coastal Engineering*, *58*, 992–1012.